231

Jordanian Journal of Computers and Information Technology (JJCIT), Vol. 05, No. 03, December 2019.

3-D POLARIZED CHANNEL MODELING FOR MULTIPOLARIZED UCA-MASSIVE MIMO SYSTEMS IN UPLINK TRANSMISSION

Abdelhamid Riadi[1], Mohamed Boulouird[1, 2] and Moha M'Rabet Hassani[1]

ABSTRACT

In this paper, a novel design of a Uniform Circular Array Massive-Multiple Input Multiple Output (UCA-mMIMO) system based on Spherical Wave (SW) is proposed in Uplink (UL) transmission. A three-dimensional (3-D) channel pattern is established and estimated, where channel orthogonality of multipolarized/unipolarized UCA-mMIMO systems is analyzed. Multipolarized and unipolarized systems are evaluated to decrease channel orthogonality. The Azimuth Angle of Arrival (AAoA) and Elevation Angle of Arrival (EAoA), as well as antenna spacing and cross-polarization discrimination, are taken into consideration. Using Monte Carlo simulation method, the results show that the multipolarized UCA-mMIMO system provides a better performance compared to the unipolarized UCA-mMIMO system in different situations. The proposed design is homely to be realized in real environment in conformance to the parameters analyzed; in order to confirm that it will be a very good choice.

KEYWORDS

Massive MIMO system, Channel orthogonality, Channel estimation, Multipolarized, Unipolarized, OSIC detector.

1. INTRODUCTION

Massive MIMO system is one of the successful technologies for the new-generation 5G. High-quality communication represented in features such as voice, audiovisual communication …etc., is promoted by using mMIMO systems, in addition to that the growing number of terminals requires a high throughput [1]. Furthermore, several publications have appeared in recent years focusing on spectral efficiency enhancement in wireless communication [2]-[4]; collecting mMIMO with Orthogonal Frequency Division Multiplexing (OFDM) can support high spectrum efficiency [5]. In the same way, the compromise between energy efficiency and spectral efficiency; measured in terms of (bits/j) and (bits/channel use/terminal), respectively, is derived using the convex optimization theory [4], where this trade-off is quantified in the case of a channel model that contains small-scale fading. Otherwise, the classical MIMO (i.e., 4G) system has a tendency to use four or eight antennas, while in mMIMO system, especially in a single cell, Base Station (BS) antennas are larger than several terminals [1]-[2], [6]. Additionally, the channel between the transceiver is an important element in mMIMO system. Due to various phenomena, such as diffraction, interference, reflection, …etc., the system performance is degraded. In the past decade, a lot of research has attracted attention to investigate perfect/imperfect Channel State Information (CSI) [7]. In the same way, when the CSI is unfinished at the BS antennas, the data detection contains erroneous bits and the system performance is deteriorated. Accordingly, various works focused on investigating the channel estimation phenomenon, in which Least-Square Channel Estimation (LSCE) is used for its simplicity and low complexity [1], [8], on the one hand. On the other hand, linear detectors, such as Zero Forcing (ZF) and Minimum Mean-Square Error (MMSE), are widely used to detect the stream data [1], [8]-[11]. Moreover, Ordered Successive Interference Cancellation (OSIC) is generally better than simple linear detectors (i.e., ZF, MMSE) [1]. Therefore, OSIC is evaluated under various criteria, such as declining Signal-to-Noise-Ratio (SNR) criterion [12] and greatest SNR criterion [13]. In addition to that, favorable propagation (i.e., channel orthogonality) is one of leading properties in mMIMO system [1]. Moreover, low channel orthogonality for different 3-D channel models has been investigated with Uniform Linear Array

1. A. Riadi, M. Hassani and M. Boulouird are with Instrumentation, Signals and Physical Systems (I2SP), Faculty of Sciences Semlalia Cadi Ayyad University, Marrakech, Morocco, E-mail: abdelhamid.riadi@edu.uca.ac.ma
2. M. Boulouird is with National School of Applied Sciences of Marrakech (ENSA-M), Cadi Ayyad University, Marrakech, Morocco, E-mail: m.boulouird@uca.ac.ma

(ULA), Uniform Rectangular Array (URA) and UCA-mMIMO using Plane Wave (PW) in many situations [14]. Similarly, PW and SW are discussed for 3-D ULA m-MIMO [15]. Furthermore, in this work, our contributions are summarized as follows:

- A new geometrical conception is realized for multipolarized UCA-mMIMO system using SW;
- A 3-D channel pattern with various parameters is modeled and estimated.

The remainder of the paper is organized as follows. In Section 2, the mMIMO model is presented in Uplink (UL) transmission, where single cell is considered. Section 3 describes the outlines of LSCE. Channel modeling for UCA-mMIMO using SW is evaluated for both multipolarized/unipolarized antennas in Section 4. In Section 5, the OSIC detector is discussed based on ZF and MMSE detectors. Section 6 presents the simulation and analysis results. Section 7 summarizes the results of this paper and draws conclusions.

2. MASSIVE MIMO MODEL

In this section, a Massive-MIMO-OFDM system is considered in Uplink transmission from N_t terminals with single antennas to a single BS with N_r antennas. The studied system is gived in Figure 1. The length of sub-carriers and the cyclic prefix (CP) are defined by K and ν, respectively. The CP is inserted on each transmitting antenna to achieve a full OFDM symbol. In this paper, the CP is superior to the utmost multi-path delay [1], [8] and [16]-[17].
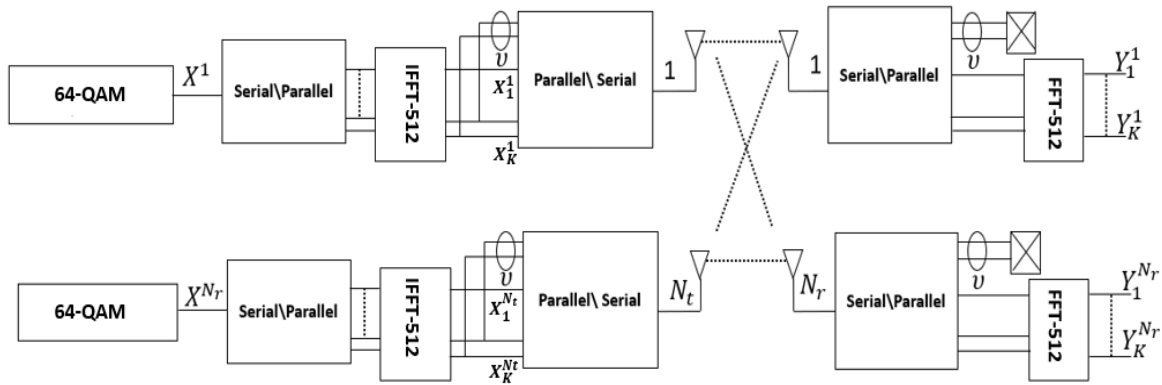

Figure 1. System model.

In the same way, at the reception side, the CP is removed on each receiving antenna. Taking-for example-the qth receiving antenna, the received signal vector $y^q(n)$ is K×1 and can be expressed as follows:

$$y^q(n) = \sum_{r=1}^{N_t} H_{cir}^{q,r} F^H X^r(n) + z^q(n) \qquad (1)$$

From Equation 1, the circulant matrix $H_{cir}^{q,r}$ has a first column defined by $[\hbar^{q,r^T}, 0_{1 \times (K-L)}]^T$, in addition to that L is the length of the channel impulse response and $\hbar^{q,r}$ represents the L×1 vector. The OFDM vector that is transmitted on each transmitting antenna is defined by $X^r(n)$ with K×1 dimensions, r and n are indices of number of transmitting antenna and time, respectively. $z^q(n)$ is the additive Gaussian noise at Time Index (TI) n with zero mean and a variance of σ_n^2. Moreover, the unitary DFT matrix with dimensions K×K is presented by F. From the eigenvalue decomposition, the circulant matrix becomes $H_{cir}^{q,r} = F^H diag\{\sqrt{K}F[\hbar^{q,r^T}, 0_{1 \times (K-L)}]^T\}F$ [1], [8] and [17]. Finally, the FFT of the received signal $y^q(n)$ is given as follows:

$$Y^q(n) = \sum_{r=1}^{N_t} diag\{\sqrt{K}F[\hbar^{q,r^T}, 0_{1 \times (K-L)}]^T\}$$
$$\times X^r(n) + \Xi^q(n) \qquad (2)$$

where, $\Xi^q(n) = Fz^q(n)$.

3. LEAST SQUARE MASSIVE MIMO

Based on the same system presented in Figure 1, the LSCE scheme is presented. Then, Equation 2 can be written as:

$$Y^q(n) = \sum_{r=1}^{Nt} diag\{X^r(n)\}F\mathfrak{h}^{q,r} + \Xi^q(n)$$
$$= \sum_{r=1}^{Nt} (diag\{D^r(n)\} + diag\{B^r(n)\})F\mathfrak{h}^{q,r} + \Xi^q(n) \tag{3}$$

From Equation 3, F is $\sqrt{K} \times l$ of F, where l is the 1st column of F, noting that $D^r_{diag}(n) = diag\{D^r(n)\}$ and $B^r_{diag}(n) = diag\{B^r(n)\}$, where $D^r_{diag}(n)$ and $B^r_{diag}(n)$ are $K \times 1$ data vector and $K \times 1$ pilot sequence vector, respectively. Hence, Equation 3 becomes:

$$Y^q(n) = \sum_{r=1}^{Nt} D^r_{diag}(n)F\mathfrak{h}^{q,r} + \sum_{r=1}^{Nt} B^r_{diag}(n)F\mathfrak{h}^{q,r} + \Xi^q(n) \tag{4}$$

Furthermore, in this work, the training of all OFDM symbols is done at maximum value of g and TI is $n \in \{0, \cdots, g-1\}$ [1], [8]. We consider the data model:

$$Y^q = T\mathfrak{h}^q + A\mathfrak{h}^q + \Xi^q \tag{5}$$

where, $Y^q = [Y^{q^T}(0), \cdots, Y^{q^T}(g-1)]^T$, $\Xi^q = [\Xi^{q^T}(0), \cdots, \Xi^{q^T}(g-1)]^T$,

$$A = \begin{bmatrix} B^1_{diag}(0)F & \cdots & B^{Nt}_{diag}(0)F \\ \vdots & & \vdots \\ B^1_{diag}(g-1)F & \cdots & B^{Nt}_{diag}(g-1)F \end{bmatrix} \quad T = \begin{bmatrix} D^1_{diag}(0)F & \cdots & D^{Nt}_{diag}(0)F \\ \vdots & & \vdots \\ D^1_{diag}(g-1)F & \cdots & D^{Nt}_{diag}(g-1)F \end{bmatrix} \tag{6}$$

and $\mathfrak{h}^q = [\mathfrak{h}^{q,1^T}, \cdots, \mathfrak{h}^{q,Nt^T}]^T$.

The LSCE technique minimizes the noise defined in Equation 5 [1], [8], based on the cost function (Equation 7), to obtain the estimated channel noted by $\hat{\mathfrak{h}}^q$

$$J(\hat{\mathfrak{h}}^q) = ||Y^q - A\hat{\mathfrak{h}}^q||^2 \tag{7}$$
$$= (Y^q - A\hat{\mathfrak{h}}^q)^H(Y^q - A\hat{\mathfrak{h}}^q)$$
$$= Y^{q^H}Y^q - Y^{q^H}A\hat{\mathfrak{h}}^q - \hat{\mathfrak{h}}^{q^H}A^HY^q + \hat{\mathfrak{h}}^{q^H}A^HA\hat{\mathfrak{h}}^q$$

Next, we take the derivation of Equation 7 relative to $\hat{\mathfrak{h}}^q$ variable,

$$\frac{\partial J(\hat{\mathfrak{h}}^q)}{\partial \hat{\mathfrak{h}}^q} = 2 * (-(A^HY^q)^* + (A^HA\hat{\mathfrak{h}}^q)^*) = 0 \tag{8}$$

Finally, we have $A^HA\hat{\mathfrak{h}}^q = A^HY^q$ and the solution of the LSCE is given by the following expression:

$$\hat{\mathfrak{h}}^q = A^+Y^q \tag{9}$$

where, A^+ is the pseudo-inverse that is equal to $(A^HA)^{-1}A^H$ if $gK \geqslant LN_t$. Because $rank(A) = min(gK, LN_t)$, the necessary and sufficient condition to have unique LSCE is $gK \geqslant LN_t$. This LS method presents low complexity and high simplicity. In addition, taking the information about the channel and the noise is not necessary [1], [8] and [17]-[19]. From Equation 5, we then find that:

$$\hat{\mathfrak{h}}^q = \mathfrak{h}^q + A^+T\mathfrak{h}^q + A^+\Xi^q \tag{10}$$

Further, to suppress the interference due to the data, the following condition is imposed:

$$A^+T = 0_{LN_t \times LN_t} \tag{11}$$

Furthermore, satisfying this condition requires choosing disjoint sets of pilot tones for training and data in each OFDM symbol (i.e., zeros in $B^r(n)$, where $D^r(n)$ contains non-zeros and inversely). Equation 10 then becomes:

$$\hat{\mathfrak{h}}^q = \mathfrak{h}^q + A^{\dagger}\Xi^q \tag{12}$$

Equation 12 is an association of two parts; the first is the true channel $\mathfrak{h}^q$ and the second is the noise in the system. Thus, for zero-mean noise, $\varepsilon\{\hat{\mathfrak{h}}^q\} = \mathfrak{h}^q + A^{\dagger}\varepsilon\{\Xi^q\} = \mathfrak{h}^q$, (i.e., $\hat{\mathfrak{h}}^q$ forms an unbiased estimate of $\mathfrak{h}^q$). Furthermore, the estimated channel matrix $\hat{\mathbb{H}} \in \mathbb{C}^{N_r \times N_t}$ which includes all terminal antennas N_t and all BS antennas N_r is given by:

$$\hat{\mathbb{H}} = \begin{bmatrix} \hat{\mathfrak{h}}^{1,1} & \cdots & \hat{\mathfrak{h}}^{1,N_t} \\ \vdots & & \vdots \\ \hat{\mathfrak{h}}^{q,1} & \cdots & \hat{\mathfrak{h}}^{q,N_t} \\ \vdots & & \vdots \\ \hat{\mathfrak{h}}^{N_r,1} & \cdots & \hat{\mathfrak{h}}^{N_r,N_t} \end{bmatrix} \tag{13}$$

where the estimated channel vector at terminal position i is given by $\hat{\mathcal{H}}_i = [\hat{\mathfrak{h}}^{1,i^T}, \cdots, \hat{\mathfrak{h}}^{N_r,i^T}]^T$.

4. CHANNEL MODELING

In this section, the UCA-mMIMO system based on SW is investigated as shown in Figure 2. Form this configuration, the horizontally polarized antenna A_1 is considered as a reference. In addition to that, all the odd ciphered antennas are horizontally polarized antennas and all the even ciphered antennas are vertically polarized antennas. Note that d is the distance between two adjacent antennas. From Figure 2, $\theta = \frac{2\pi}{N_r}$, $\theta_2 = \theta$, $\theta_3 = 2\theta$, $\cdots$, $\theta_m = (m-1)\theta$ and the radius r is equal to $\frac{d}{2\sin(\frac{\theta}{2})}$.

Similarly, the signals arrive from the S location; also, $S_1, S_2, \cdots, S_m$ are successive projections of S on the horizontal planes $x - A_1 - y, x - A_2 - y, \cdots, x - A_m - y$, respectively. Each projection has a distance from the source S noted by $h = h_1, h_2, \cdots, h_m$, respectively. $d_{x_1}, d_{x_2}, \cdots, d_{x_m}$ are the projections on the x axis of $S_1, S_2, \cdots, S_m$, respectively, while d_y denotes their projections on the y axis.
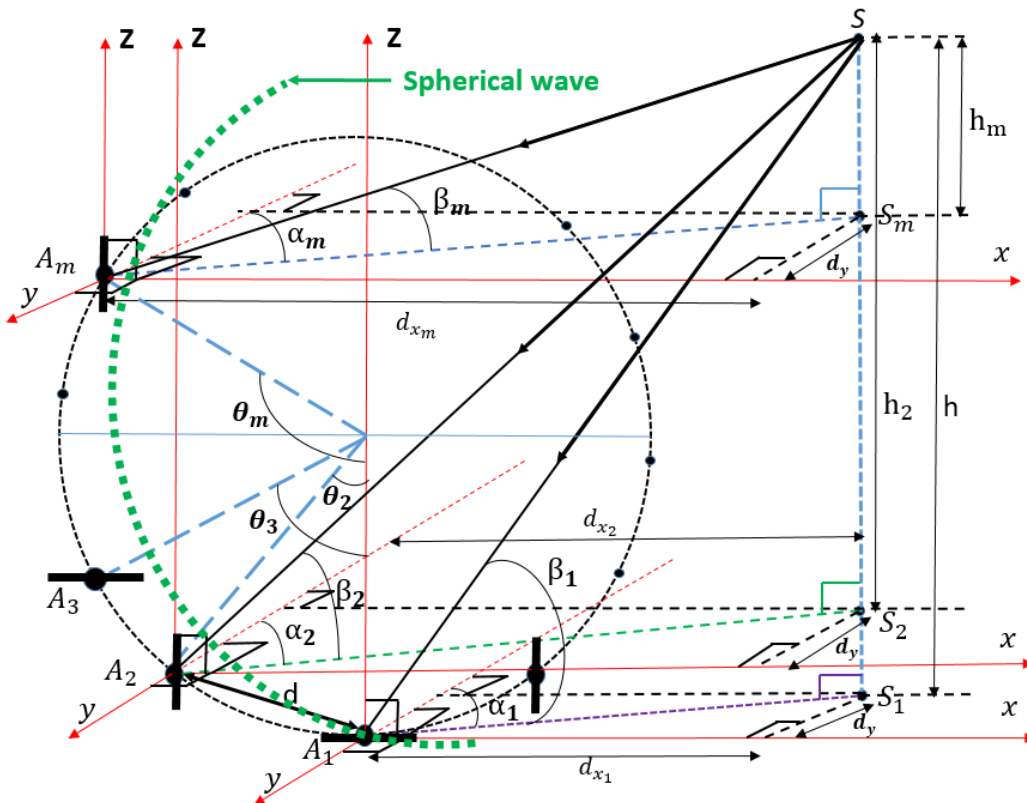

Figure 2. Multipolarized uniform circular array Massive-MIMO configuration.

Otherwise, the distance between each antenna and the source S can be defined by:

$$d_{SA_1} = \sqrt{d_{x_1}^2 + d_y^2 + h_1^2} \tag{14}$$

$$d_{SA_2} = \sqrt{(d_{x_1} + r * sin(\theta))^2 + d_y^2 + h_2^2} \tag{15}$$

$$d_{SA_m} = \sqrt{(d_{x_1} + r * sin((m-1)\theta))^2 + d_y^2 + h_m^2} \tag{16}$$

$$d_{SA_{N_r}} = \sqrt{(d_{x_1} + r * sin((N_r-1)\theta))^2 + d_y^2 + h_{N_r}^2} \tag{17}$$

Depending on the geometrical relationship presented in Figure (2), for an arbitrary antenna, we have:

$$d_{x_1} = d_y * tan(\alpha_1) \tag{18}$$

$$h_m = tan(\beta_m) * \sqrt{d_y^2 + d_y^2 * tan(\alpha_m)^2} \tag{19}$$

In addition to that, the antenna A_1 is considered as a reference antenna. The estimated path of multipath channels at terminal position i and at BS antennas A_1 and A_m using SW can be expressed by:

$$\hat{\mathfrak{h}}_{UCA}^{1,i} = \sqrt{P_H}e^{j(\phi_i + 2\pi\sqrt{d_{x_{1,i}}^2 + d_{y,i}^2 + h_{1,i}^2}/\lambda)} \tag{20}$$

$$\hat{\mathfrak{h}}_{UCA}^{m,i} = \sqrt{P_V}e^{j(\phi_i + 2\pi\sqrt{(d_{x_{1,i}} + r*sin((m-1)\theta))^2 + d_{y,i}^2 + h_{m,i}^2}/\lambda)} \tag{21}$$

where, P_H and P_V are the horizontally polarized power and vertically polarized power in this path, respectively. λ is the wavelength and ϕ is the uniform random phase as assumed by IID on $[-\pi, \pi)$ [14].

Otherwise, the uniform distribution of AAS and EAS is used to describe the AAoA and EAoA distribution. In this paper, α and β represent AAS and EAS, respectively; several authors [14], [20] have established the Power Azimuth Spread (PAS) to explain the AAoA/EAoA as follows:

$$p(Y) = \frac{1}{2\Delta Y}, \quad -\Delta Y + Y_0 \leqslant Y \leqslant \Delta Y + Y_0, \tag{22}$$

where, Y_0 and ΔY are the mean of AAoA/EAoA and AAS/EAS, respectively.

Moreover, in real environment and thanks to the multipath phenomenon, polarization can be changed between the terminal and the BS antennas. Thereby, to characterize this phenomenon, cross-polarization discrimination (XPD) is expressed as [14], [25]:

$$XPD = \frac{E\{|\mathfrak{h}_{VV}|^2\}}{E\{|\mathfrak{h}_{VH}|^2\}} = \frac{E\{|\mathfrak{h}_{HH}|^2\}}{E\{|\mathfrak{h}_{HV}|^2\}} = \frac{1-a}{a}, \tag{23}$$

where, $E\{\}$ describes the expectation operator, $\mathfrak{h}_{VV}/\mathfrak{h}_{HH}$ and $\mathfrak{h}_{VH}/\mathfrak{h}_{HV}$ are the channels between transceivers with the same polarization and with different polarizations, respectively. Then, Equations 20 and 21 can be written as:

$$\hat{\mathfrak{h}}_{UCA,XPD}^{1,i} = \sqrt{P_V a + P_H(1-a)}e^{j(\phi_i + 2\pi\sqrt{d_{x_{1,i}}^2 + d_{y,i}^2 + h_{1,i}^2}/\lambda)} \tag{24}$$

$$\hat{\mathfrak{h}}_{UCA,XPD}^{m,i} = \sqrt{P_H a + P_V(1-a)}e^{j(\phi_i + 2\pi\sqrt{(d_{x_{1,i}} + r*sin((m-1)\theta))^2 + d_{y,i}^2 + h_{m,i}^2}/\lambda)} \tag{25}$$

Furthermore, in this paper and in related references [14], [21]-[24], $a(0 < a \leq 1)$ represents the power that is seeped in the UL transmission from the vertically/horizontally polarized terminal to the horizontally/vertically polarized BS antenna; in the case where there is no seepage, a is equal to 0. In

addition to that, $P_X(1-a)$ is the power kept in similar transmission and reception polarization states, where $P_X a$ is the power seepage to transmission in one polarization state and to reception in the orthogonal polarization state ($X \in V, H$).

From our proposed configuration, Equations 24 and 25 can be generalized for all multipaths at terminal position e with single horizontally polarized antenna side and f with single vertically polarized antenna side, over all BS antennas (i.e., $\{1, \cdots, N_r\}$) basing on SW by:

$$\widehat{\mathcal{H}}_e^{UCA,XPD} = \begin{bmatrix} \widehat{\mathfrak{h}}_{UCA,XPD}^{1,e} \\ \widehat{\mathfrak{h}}_{UCA,XPD}^{2,e} \\ \vdots \\ \widehat{\mathfrak{h}}_{UCA,XPD}^{m,e} \\ \widehat{\mathfrak{h}}_{UCA,XPD}^{m+1,e} \\ \vdots \\ \widehat{\mathfrak{h}}_{UCA,XPD}^{N_r,e} \end{bmatrix} = \begin{bmatrix} \sqrt{P_H(1-a)}\,e^{j(\phi_e+2\pi\sqrt{d_{x_1,e}^2+d_{y,e}^2+h_{1,e}^2}/\lambda)} \\ \sqrt{P_H(a)}\,e^{j(\phi_e+2\pi\sqrt{(d_{x_1,e}+r*sin(\theta))^2+d_{y,e}^2+h_{2,e}^2}/\lambda)} \\ \vdots \\ \sqrt{P_H(a)}\,e^{j(\phi_e+2\pi\sqrt{(d_{x_1,e}+r*sin((m-1)\theta))^2+d_{y,e}^2+h_{m,e}^2}/\lambda)} \\ \sqrt{P_H(1-a)}\,e^{j(\phi_e+2\pi\sqrt{(d_{x_1,e}+r*sin((m)\theta))^2+d_{y,e}^2+h_{m+1,e}^2}/\lambda)} \\ \vdots \\ \sqrt{P_H(a)}\,e^{j(\phi_e+2\pi\sqrt{(d_{x_1,e}+r*sin((N_r-1)\theta))^2+d_{y,e}^2+h_{N_r,e}^2}/\lambda)} \end{bmatrix}. \quad (26)$$

$$\widehat{\mathcal{H}}_f^{UCA,XPD} = \begin{bmatrix} \widehat{\mathfrak{h}}_{UCA,XPD}^{1,f} \\ \widehat{\mathfrak{h}}_{UCA,XPD}^{2,f} \\ \vdots \\ \widehat{\mathfrak{h}}_{UCA,XPD}^{m,f} \\ \widehat{\mathfrak{h}}_{UCA,XPD}^{m+1,f} \\ \vdots \\ \widehat{\mathfrak{h}}_{UCA,XPD}^{N_r,f} \end{bmatrix} = \begin{bmatrix} \sqrt{P_V(a)}\,e^{j(\phi_f+2\pi\sqrt{d_{x_1,f}^2+d_{y,f}^2+h_{1,f}^2}/\lambda)} \\ \sqrt{P_V(1-a)}\,e^{j(\phi_f+2\pi\sqrt{(d_{x_1,f}+r*sin(\theta))^2+d_{y,f}^2+h_{2,f}^2}/\lambda)} \\ \vdots \\ \sqrt{P_V(1-a)}\,e^{j(\phi_f+2\pi\sqrt{(d_{x_1,f}+r*sin((m-1)\theta))^2+d_{y,f}^2+h_{m,f}^2}/\lambda)} \\ \sqrt{P_V(a)}\,e^{j(\phi_f+2\pi\sqrt{(d_{x_1,f}+r*sin((m)\theta))^2+d_{y,f}^2+h_{m+1,f}^2}/\lambda)} \\ \vdots \\ \sqrt{P_V(1-a)}\,e^{j(\phi_f+2\pi\sqrt{(d_{x_1,f}+r*sin((N_r-1)\theta))^2+d_{y,f}^2+h_{N_r,f}^2}/\lambda)} \end{bmatrix}. \quad (27)$$

From Equations 26 and 27, P_H and P_V are the horizontally and vertically polarized power of terminals e and f, respectively. In this paper, after getting the estimated channel vectors of terminal e with single horizontally polarized antenna and f with vertically polarized antenna for UCA-mMIMO systems in Equations 26 and 27, the channel orthogonality between $\widehat{\mathcal{H}}_e^{UCA,XPD}$ and $\widehat{\mathcal{H}}_f^{UCA,XPD}$ is defined by [14], [26]-[27]:

$$\delta_{e,f} = \frac{|(\widehat{\mathcal{H}}_e^{UCA,XPD})^H \widehat{\mathcal{H}}_f^{UCA,XPD}|}{\|\widehat{\mathcal{H}}_e^{UCA,XPD}\|.\|\widehat{\mathcal{H}}_f^{UCA,XPD}\|} \quad (28)$$

where, $\|.\|$ represents the Euclidean norm. Similarly, the estimated channel matrix (13) can be rewritten as $\widehat{\mathbb{H}} = [\widehat{\mathcal{H}}_1^{UCA,XPD}, \cdots, \widehat{\mathcal{H}}_e^{UCA,XPD}, \cdots, \widehat{\mathcal{H}}_f^{UCA,XPD}, \cdots, \widehat{\mathcal{H}}_{N_t}^{UCA,XPD}]$; where, the estimated vector at terminal position i is noted by $\widehat{\mathcal{H}}_i^{UCA,XPD} = [\widehat{\mathfrak{h}}_{UCA,XPD}^{1,i}{}^T, \cdots, \widehat{\mathfrak{h}}_{UCA,XPD}^{N_r,i}{}^T]^T$. In the same way, according to literature, the authors of [14] and [28] supposed that a half of the terminals are horizontally polarized antennas and the other half of the terminals are vertically polarized antennas at a short time due to arbitrary location.

5. OSIC SIGNAL DETECTION

In this part of the paper, we present an important class of nonlinear signal detection, specifically the OSIC [1], [8]-[9]. Hence, according to Figure 3, we illustrate the OSIC signal detection for an example of three spatial streams. Furthermore, for symbol detection, the Linear Transformation Matrix (LTM), defined as $T_{ZF} = (\widehat{\mathbb{H}}^H \widehat{\mathbb{H}})^{-1} \widehat{\mathbb{H}}^H$ [9]-[11], [29], is taken into account. Moreover, the first data is detected with the first row vector of LTM (i.e., T_{ZF}); after the slicing process is carried out, x_1 is created. The interference due to the detected stream in the first stage is subtracted from the received signal; that is $y_1 = y - \widehat{\mathcal{H}}_1^{UCA,XPD} x_1$, where $y = [Y^1, \cdots, Y^q, \cdots, Y^{N_r}]^T$. Hence, the interference from the first stage is canceled; in addition to that, another stream is detected and sliced in the second stage x_2 and the interference is canceled by $y_2 = y_1 - \widehat{\mathcal{H}}_2^{UCA,XPD} x_2$. In the same way, detection and slicing of the stream as well as the interference cancellation steps are carried out in each stage [1], [8] and [29]-[32].
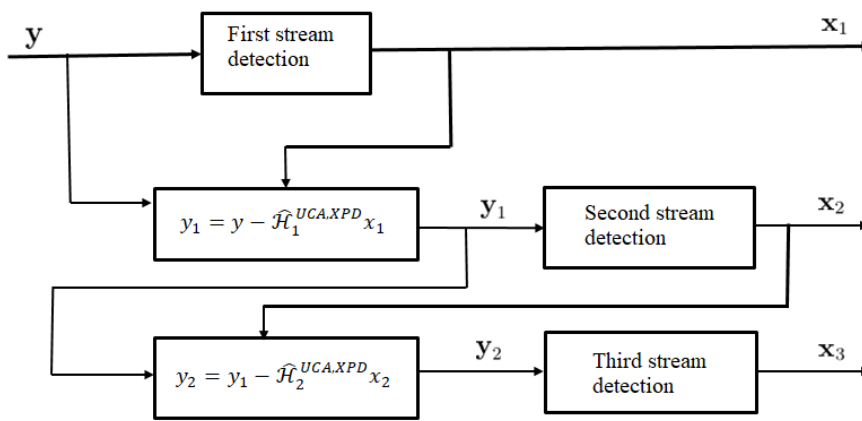

Figure 3. Explanation of OSIC signal detection, an example of three transmitting antennas.

Otherwise, if the process of canceling the interference is done with an erroneous decision in any stage, error propagation will spread in the following stage by order of detection. Hence, next in this section, we describe two methods for reducing error propagation.

• SINR-Based Ordering (SINR-BO): in this case, the stream with big post detection Signal-to-Interference-plus-Noise-Ratio (SINR) is detected first [1]. Based on the transformation matrix $T_{MMSE} = (\widehat{\mathbb{H}}^H \widehat{\mathbb{H}} + 2\sigma_n^2 I)^{-1} \widehat{\mathbb{H}}^H$, the post detector with SINR is defined as:

$$SINR_i = \frac{E_x |T_{i,MMSE} \widehat{\mathcal{H}}_i^{UCA,XPD}|^2}{E_x \sum_{l \neq i} |T_{i,MMSE} \widehat{\mathcal{H}}_l^{UCA,XPD}|^2 + \sigma_n^2 \|T_{i,MMSE}\|^2} \tag{29}$$

where, $i = 1, 2, \cdots, N_t$ and E_x transmitted signal energy. $T_{i,MMSE}$ is the ith row of T_{MMSE} and $\widehat{\mathcal{H}}_i^{UCA,XPD}$ is the ith column vector of the estimated channel matrix $\widehat{\mathbb{H}}$. In fact, once the N_t of SINR are calculated based on T_{MMSE}, we extract the equivalent stage with the maximum SINR. In addition to that, the procedure discussed above is applied for symbol detection. Furthermore, T_{MMSE} is modified by suppression of the channel gain vector equivalent to the data detected. Otherwise, the computational complexity of all numbers of SINR is given by $\sum_{i=1}^{N_t} i = \frac{N_t(N_t+1)}{2}$.

• SNR-Based Ordering (SNR-BO): in this method, higher Signal-to-Noise-Ratio (SNR) is detected first [1]. Similarly based on the transformation matrix T_{ZF}, SNR is defined as:

$$SNR_i = \frac{E_x}{\sigma_n^2 \|T_{i,ZF}\|^2} \tag{30}$$

where, $i = 1, 2, \cdots, N_t$. Similarly, the procedure discussed in the first method can be used. Otherwise, the computational complexity of all numbers of SNR is giving by $\sum_{i=1}^{N_t} i = \frac{N_t(N_t+1)}{2}$ [1].

6. SIMULATION RESULTS

In the next part of this paper, a set of performance results is discussed. According to Figure 1, the length of OFDM subcarriers is equal to 512 and the CP is 128; the higher order modulation QAM is taken equal to 64, the g consecutive OFDM symbol is set to 100 and the number of taps is supposed equal to 1. Furthermore, based on LSCE method (Section 3), the estimated channel is evaluated. Our proposed UCA-mMIMO system is analyzed for 10000 samples of the channel based on Monte Carlo simulation and the power is normalized. Moreover, Figure 4 depicts channel orthogonality (i.e., favorable propagation) for the UCA-mMIMO system on the one hand. On the other hand, the XPD is set to be 8 dB and the mean of AAoA/EAoA is equal to 0Â°; the distance between the terminal and the BS antenna is set to be 200λ. Similarly to some reports in the literature [5], [33]-[35], the antenna spacing is equal to 0.5λ.
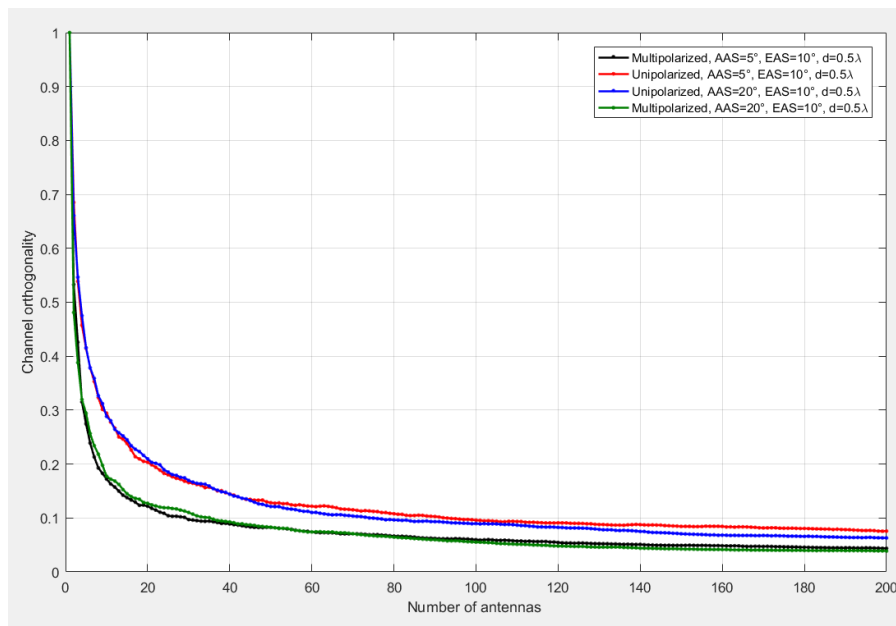

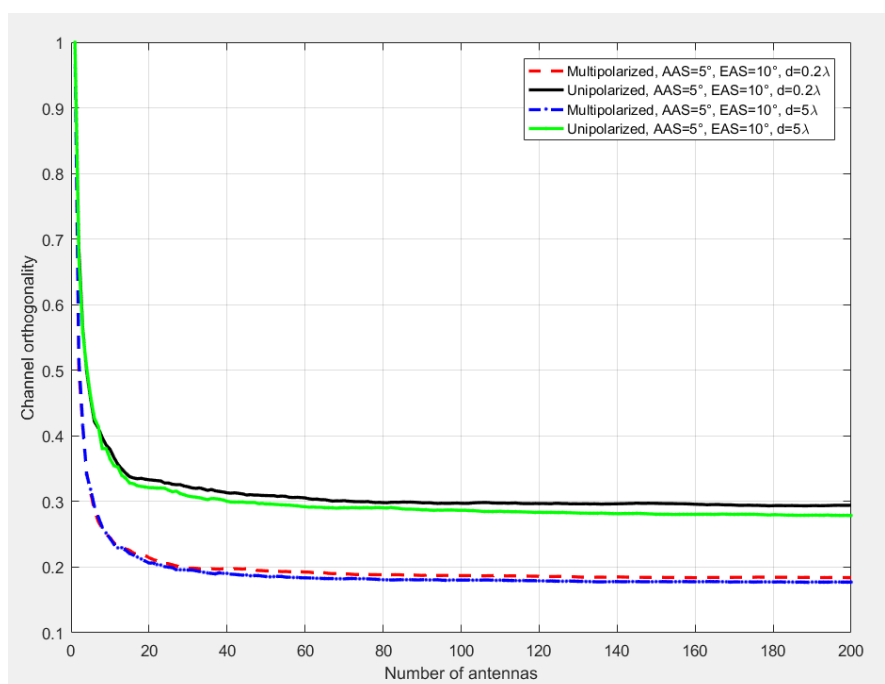Figure 4. Channel orthogonality *vs.* number of antennas with different AAS.

Figure 5. Channel orthogonality *vs.* number of antennas with different antenna spacings.

239

Jordanian Journal of Computers and Information Technology (JJCIT), Vol. 05, No. 03, December 2019.

From Figure 4, it has been found that channel orthogonality of multipolarized/unipolarized systems decreases when the number of antennas increases. In the case when AAS=5Â° (i.e., poor scattering) and $N_r = 20$, channel orthogonality is nearly 0.2 for unipolarized systems; while it's nearly 0.12 for multipolarized systems; in the same way, when AAS=20Â° (i.e., rich scattering) and $N_r = 200$, channel orthogonality is nearly 0.06 for unipolarized systems, while it's nearly 0.03 for multipolarized ones. Consequently, channel orthogonality is affected by AAS, while the effect of EAS is negligible. In addition to that, using multipolarized UCA-mMIMO can decrease more channel orthogonality (i.e., favorable propagation) compared to unipolarized UCA-mMIMO. Hence, employing multipolarized UCA-mMIMO system in real environment can decline the necessity of rich scattering.

In the next part of this paper, AAS is equal to $5Â°$ and EAS is equal to $10Â°$. Also, XPD is set to be 8 dB. Figure 5 shows that channel orthogonality declines as the BS antenna spacing (i.e., N_r) increases. In the case with $N_r = 20$ and $d = 0.2\lambda$ (i.e., small antenna spacing), channel orthogonality is nearly 0.33 with unipolarized antennas, while it's nearly 0.21 for multipolarized antennas. Moreover, when $N_r = 200$, channel orthogonality is nearly 0.29 with unipolarized antennas and it's about 0.18 with multipolarized antennas. Otherwise, when $d = 5\lambda$ (i.e., large antenna spacing) the multipolarized antennas decline more channel orthogonality compared to unipolarized antennas. Hence, using small antenna spacing and multipolarized UCA-mMIMO can help decrease channel orthogonality between terminals and reduce the need of a large antenna spacing.
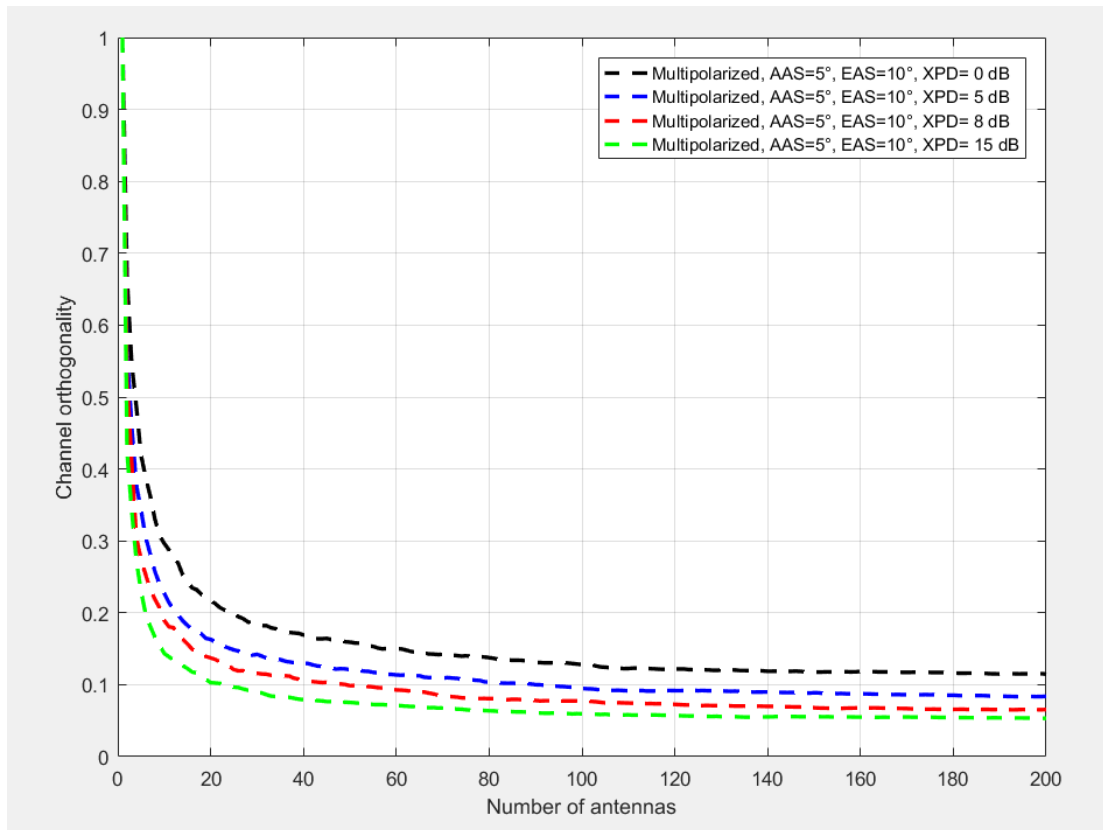

Figure 6. Channel orthogonality *vs.* number of antennas with different XPD.

Otherwise, in the case of poor scattering (i.e., AAS=5Â°) and an antenna spacing kept at the same value (0.5λ), the Figure 6 shows channel orthogonality of multipolarized UCA-mMIMO system; it has been found that when $N_r = 20$, channel orthogonality is nearly 0.22 with $XPD = 0$ dB and it's nearly 0.1 with $XPD = 15$ dB. When the BS antenna $N_r = 200$, channel orthogonality with $XPD = 0$ is nearly 0.12, while it's lower than 0.05 with $XPD = 15$ dB. Furthermore, an increase of XPD declines more channel orthogonality, thus more power is kept in the similar transmitting and receiving polarization states. Similarly, a large BS antenna number can help decrease channel orthogonality, specifically in a small XPD (i.e., more power seepage).

Figure 7 shows the performance results of OSIC detector using multipolarized/unipolarized UCA-mMIMO system. AAS is equal to 5Â° and EAS is equal to 10Â°; XPD is set to 8 dB. In addition to that, $d = 0.5\lambda$ and $d_y = 200\lambda$; according to estimated matrix (25), the number of terminals (N_t) is equal to 50 and the BS antenna number (N_r) is equal to 200. From this Figure the BER decreases over the range of SNR. Furthermore, in high-SNR region, multipolarized UCA-mMIMO systems perform better than unipolarized UCA-mMIMO systems; at SNR equal to 20 dB and using $OSIC\_SINR$ based ordering, BER is equal to 21.78×10^{-3} and 20.55×10^{-4} for unipolarized and multipolarized antennas, respectively, while when $OSIC\_SNR$ based ordering is used, BER is equal to 78.98×10^{-4} and 70.94×10^{-5} for unipolarized and multipolarized antennas, respectively. Hence, multipolarized antennas outperform unipolarized antennas; in addition to that, the gaps between the true channel and multipolarized antennas using $OSIC\_SINR$ based ordering and $OSIC\_SNR$ based ordering are equal to 2 dB and 0.8 dB, respectively at $BER = 18.7 \times 10^{-4}$. Consequently, $OSIC\_SNR$ based ordering with multipolarized UCA-mMIMO system provides a better performance.
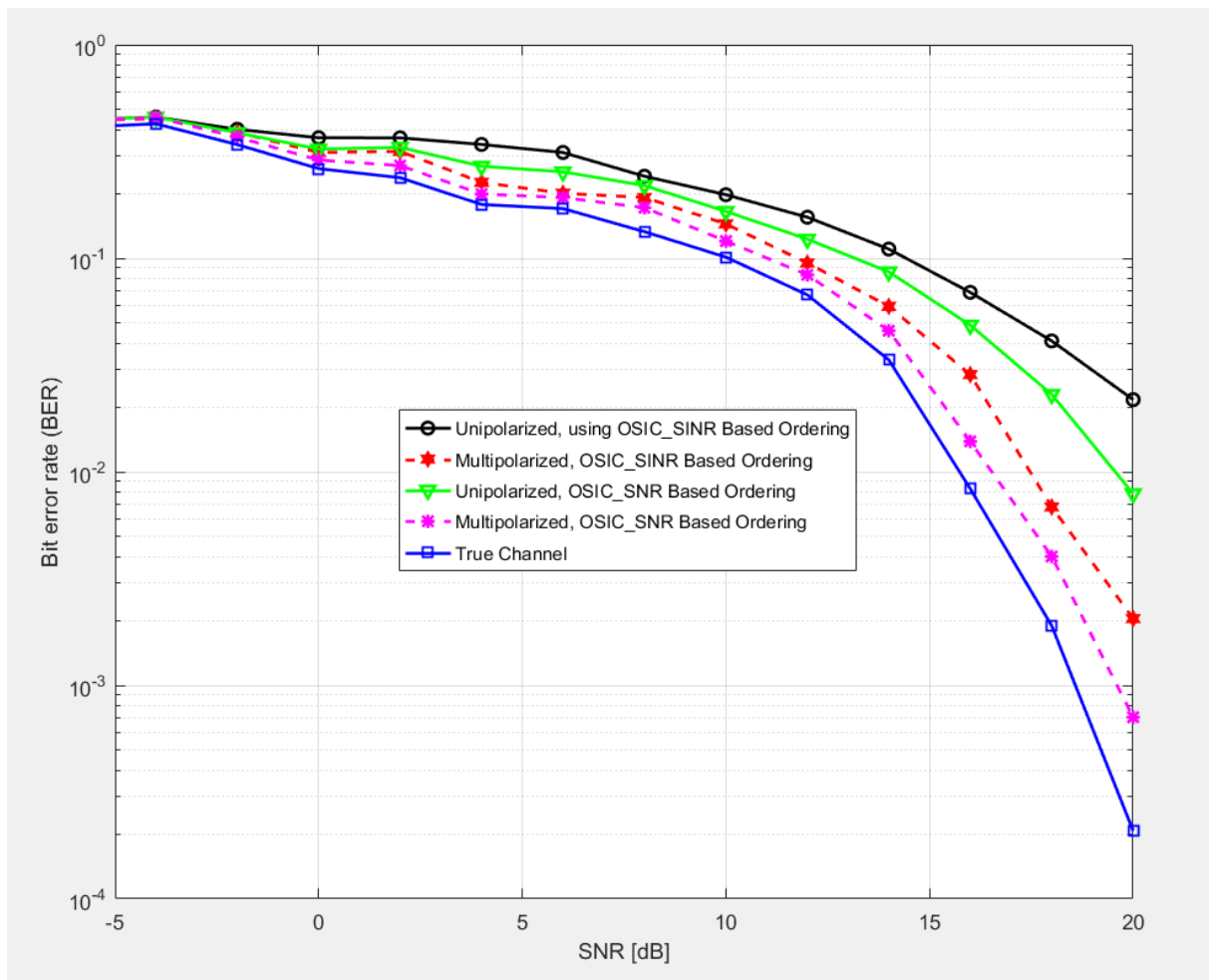

Figure 7. Bit error rate *vs.* signal to noise ratio for unipolarized/multipolarized UCA-mMIMO system with two OSIC detectors.

7. CONCLUSIONS

In this paper, UCA-mMIMO system design is proposed. A 3-D channel pattern of UCA-mMIMO is estimated using LSCE method. The presented pattern can be adjusted based on parameters analyzed. From the simulation results, it can be concluded that multipolarized UCA-mMIMO in each time declines more channel orthogonality in many situations compared to unipolarized UCA-mMIMO. Using $OSIC\_SNR$ based ordering with multipolarized UCA-mMIMO system provided a better performance compared to $OSIC\_SINR/OSIC\_SNR$ based ordering with unipolarized UCA-mMIMO

system. Summing up the results, it can be concluded that our proposed pattern using multipolarized antennas can be implemented and adapted if miniaturization of electronic elements is indispensable and would be the first candidate for Massive-MIMO systems.

REFERENCES

[1] A. Riadi, M. Boulouird and M. M. Hassani, "ZF/MMSE and OSIC Detectors for UpLink OFDM Massive MIMO systems," Proc. of the IEEE Jordan International Joint Conference on Electrical Engineering and Information Technology (JEEIT), pp. 767 – 772, 9-11 April 2019, Amman, Jordan, 2019.

[2] V. Jungnickel, K. Manolakis, W. Zirwas, B. Panzner, V. Braun, M. Lossow, M. Sternad, R. Apelfrojd and T. Svensson, "The Role of Small Cells, Coordinated Multipoint and Massive MIMO in 5G," IEEE Communications Magazine, vol. 52, no. 5, pp. 44-51, 2014.

[3] E. Bjornson, E. G. Larsson and T. L. Marzetta, "Massive MIMO: Ten Myths and One Critical Question," IEEE Communications Magazine, vol. 54, no. 2, pp. 114-123, 2016.

[4] L. Zhao, K. Li, K. Zheng and M. Omair Ahmad, "An Analysis of the Tradeoff between the Energy and Spectrum Efficiencies in an Uplink Massive MIMO-OFDM System," IEEE Transactions on Circuits and Systems, vol. 62, no. 3, pp. 291-295, 2014.

[5] F. Rusek, D. Persson, B. Kiong Lau, E. G. Larsson, T. L. Marzetta, O. Edfors and F. Tufvesson, "Scaling Up MIMO: Opportunities and Challenges with Very Large Arrays," IEEE Signal Processing Magazine, vol. 30, no. 1, pp. 40-60, January 2013.

[6] T. Van Chien and E. Björnson, "5G Mobile Communications," *Springer*, pp. 77-116, 2017.

[7] H. Quoc Ngo, E. G. Larsson, T. L. Marzetta and M. Omair Ahmad, "Energy and Spectral Efficiency of Very Large Multiuser MIMO Systems," IEEE Transactions on Communications, vol. 61, no. 4, pp. 1436 - 1449, 2013.

[8] A. Riadi, M. Boulouird and M M.Hassani, "Least Squares Channel Estimation of an OFDM Massive MIMO System for 5G Wireless Communications," in: M. Bouhlel, S. Rovetta (Eds.), Proceedings of the 8th International Conference on Sciences of Electronics, Technologies of Information and Telecommunications (SETIT'18), vol. 2, 2018, Smart Innovation, Systems and Technologies, vol. 146, Springer, Cham.

[9] S. Yang and L. Hanzo, "Fifty Years of MIMO Detection: The Road to Large-Scale MIMOs," IEEE Communications Surveys & Tutorials, vol. 17, no. 4, 2015.

[10] A. Riadi, M. Boulouird and M. M. Hassani, "An Overview of Massive-MIMO in 5G Wireless Communications," Colloque International TELECOM 2017 & 10 emes JFMMA, EMI - Rabat, Morocco, Mai 10-12, 2017.

[11] P. Rajeev, A. Prabhat and L. Norsang, "Sphere Detection Technique: An Optimum Detection Scheme for MIMO System," International Journal of Computer Applications, vol. 100, no. 2, pp. 975-987, August 2014.

[12] D. Wiibben, R. Bohnke, V. Kuhn and K.-D. Kammeyer, "MMSE Extension of V-BLAST Based on Sorted QR Decomposition," Proc. of IEEE 58th VTC-Fall, pp. 508-512, Orlando, FL, USA, Oct. 2003.

[13] R. Bohnke, D. Wubben, V. Kuhn, and K.-D. Kammeyer, "Reduced Complexity MMSE Detection for BLAST Architectures," Proc. of IEEE GLOBECOM, pp. 2258-2262, San Francisco, USA, Dec. 2003.

[14] X. Cheng, Y. He, Li Zhang and J. Qiao, "Channel Modeling and Analysis for Multipolarized Massive-MIMO Systems," International Journal of Communication Systems, vol. 21, no. 12, pp. e3703, 2018.

[15] X. Cheng and Y. He, "Channel Modeling and Analysis of ULA Massive-MIMO Systems," Proc. of the 20th International Conference on Advanced Communication Technology (ICACT), pp. 411-416, 2018.

[16] A. Moradi, H. Bakhshi and V. Najafpoor, "Pilot Placement for Time-Varying MIMO OFDM Channels with Virtual Subcarriers," Communications and Networks, vol. 3, no. 1, pp. 31-38, February 2011.

[17] I. Barhumi, G. Leus and M. Moonen, "Optimal Training Design for MIMO OFDM Systems in Mobile Wireless Channels," IEEE Signal Processing Magazine, vol. 51, no. 6, pp. 1615-1624, May 2003.

[18] T.-L. Tung, K. Yao and R. E. Hudson, "Channel Estimation and Adaptive Power Allocation for Performance Arid Capacity Improvement of Multiple-Antenna OFDM Systems," Proc. of the 3rd IEEE Workshop on Signal Processing Advances in Wireless Communications (SPAWC'01), China, 2001.

[19]   A. Youssefi and J. El-Abbadi, "Pilot-symbol Patterns for MIMO OFDM Systems under Time Varying Channels," International Conference on Electrical and Information Technologies (ICEIT), Marrakech, Morocco, March 25-27, 2015.

[20]   Y. S. Cho, J. Kim, W. Y. Yang and C. G. Kang, "MIMO-OFDM Wireless Communication Technology with MATLAB," Beijing: Publishing House of Electronics Industry, 2013.

[21]   Y. He, X. Cheng and G. L. Stuber, "On Polarization Channel Modeling," IEEE Wireless Communications, vol. 23, no. 1, pp. 80-86, February 2016.

[22]   M. Coldrey, "Modeling and Capacity of Polarized MIMO Channels," Proc. of VTC Spring 2008-IEEE Vehicular Technology Conference, pp. 440-444, May 2008.

[23]   A. Habib, B. Krasniqi and M. Rupp, "Convex Optimization for Receive Antenna Selection in Multi-Polarized MIMO Transmissions," Proc. IEEE Sys., Signals and Image Processing Conf., pp. 269-275, April 2012.

[24]   K. H. Jeon, B. Hui, K. H. Chang, H. S. Park and Y. O. Park, "SISO Polarized Flat Fading Channel Modeling for Dual-Polarized Antenna Systems," The International Conference on Information Network, pp. 368-373, Feb. 2012.

[25]   L. Jiang, L. Thiele and V. Jungnickel, "On the Modelling of Polarized MIMO Channel," Proc. Europ. Wireless, pp. 1-4, 2007.

[26]   N. H. Quoc, E. G. Larsson and T. L. Marzetta, "Aspects of Favorable Propagation in Massive-MIMO," Proceedings of the 22nd European Signal Processing Conference (EUSIPCO), pp.76-80, September 2014.

[27]   K. Zheng, S. Ou and X. Yin, "Massive-MIMO Channel Models: A Survey," International Journal of Antennas and Propagation, vol. 11, pp. 1-10, 2014.

[28]   J. Park and B. Clerckx, "Multi-user Linear Precoding for Multi-polarized Massive- MIMO System under Imperfect CSIT," IEEE Transactions on Wireless Communications, vol. 14, no. 5, pp. 2532-2547, 2015.

[29]   A. Chockalingam and B. Sundar Rajan, Large MIMO Systems, Cambridge University Press, 2014.

[30]   G. J. Foschini, "Layered Space-time Architecture for Wireless Communication in a Fading Environment When Using Multi-element Antennas," Bell Labs Technical Journal, vol. 1, no. 2, pp. 41-59, 1996.

[31]   P. W. Wolniansky, G. J. Foschini, G. D. Golden and R. A. Valenzuela, "V- BLAST: An Architecture for Realizing Very High Data Rates over the Rich-scattering Wireless Channel," Proc. of URSI International Symposium on Signals, Systems and Electronics Conference Proceedings (Cat. No.98EX167), pp. 295-300, 1998.

[32]   G. D. Golden, C. J. Foschini, R. A. Valenzuela and P. W. Wolniansky, "Detection Algorithm and Initial Laboratory Results Using V-BLAST Space-time Communication Architecture," Electronics Letters, vol. 35, no. 1, pp. 14-16, 1999.

[33]   J. Li, Y. Zhao and Z. Tan, "Indoor Channel Measurements and Analysis of a Large-scale Antenna System at 5.6 GHz," Proc. of IEEE/CIC International Conference on Communications in China (ICCC), pp. 281-285, 2014.

[34]   X. Gao, O. Edfors, F. Rusek and F. Tufvesson, "Linear Pre-coding Performance in Measured Very-Large MIMO Channels, Proc. of IEEE Vehicular Technology Conference (VTC Fall), pp.1-5, 2011.

[35]   J. Hoydis, C. Hoek, T. Wild and S. Ten Brink, "Channel Measurements for Large Antenna Arrays," Proc. of International Symposium on Wireless Communication Systems (ISWCS), pp. 811-815, 2012.

ملخص البحث:

فـي هـذه الورقـة، يـتم اقتـراح تصـميم مبنكـر لنظـام ضـخم ذي مصـفوفة دائريـة متجانسـة، متعـدد المـداخل والمخـارج، مبنـي علـى الموجـة الكرويـة، فـي الإرسـال القـائم علـى الـربط العلـوي؛ إذ يـتم إنشـاء نمـط ثلاثـي الأبعـاد للقنـوات، وتحليـل تعامُـد القنـوات فـي الأنظمـة متعـددة الاسـتقطاب والأنظمـة أحاديـة الاسـتقطاب متعـددة المـداخل والمخـارج، التـي تمتلـك مصـفوفة دائريـة متجانسـة. فقد جـرى تقيـيم أنظمـة متعـددة الاستقطاب وأخـرى أحاديـة الاستقطاب؛ مـن أجـل التقليـل مـن تعامُـد القنـوات.

وقـد تـم أخـذ كـل مـن: زاويـة سَمْت الوصـول، وزاويـة مَيْـل الوصـول، جنبـاً الـى جنـب مـع مسـافة التباعُـد بـين الهوائيـات، وتمييـز الاسـتقطاب المتقـاطع، بعـين الاعتبـار. وباسـتخدام طريقـة مونـتِ كـارلو للمحاكـاة، بينـت النتـائج أن الأنظمـة متعـددة الاسـتقطاب تعطـي أداء أفضـل إذا قورنـت بمثيلاتها من الأنظمة أحادية الاستقطاب في ظل أوضاع مختلفة.

والجـدير بالـذكر أن التصـميم المقتـرح فـي هـذه الدراسـة يتعـين تحقيقـه بشـكل بسـيط فـي بيئـة حقيقيـة تـتلاءم مـع المتغيـرات التـي خضـعت للتحليـل؛ مـن أجـل التحقـق مـن أنـه يمثـل خيـاراً جيـداً جـداً.